Research Square

Preprints are preliminary reports that have not undergone peer review.
They should not be considered conclusive, used to inform clinical practice,
or referenced by the media as validated information.

Dorsal-ventral precuneus gradients organise large-scale networks and track consciousness level

Dian Lu

d1577@zju.edu.cn

Zhejiang University

Adapa Ram

University of Cambridge https://orcid.org/0000-0002-9845-8532

Robin Carhart-Harris

University of California San Francisco https://orcid.org/0000-0002-6062-7150

Leor Roseman

Imperial College London https://orcid.org/0000-0001-9990-6029

Adrian Owen

Western University

Lorina Naci

Trinity College Dublin https://orcid.org/0000-0001-9630-3978

David Menon

University of Cambridge https://orcid.org/0000-0002-3228-9692

Emmanuel Stamatakis

University of Cambridge https://orcid.org/0000-0001-6955-9601

Article

Keywords:

Posted Date: March 6th, 2026

DOI: https://doi.org/10.21203/rs.3.rs-8883514/v1

License: This work is licensed under a Creative Commons Attribution 4.0 International License.
Read Full License

Additional Declarations: There is **NO** Competing Interest.

Dorsal–ventral precuneus gradients organise large-scale networks and track consciousness level

Dian Lyu[1,2], Ram Adapa[3], Robin L. Carhart-Harris[5], Leor Roseman[6], Adrian M. Owen[7], Lorina Naci[8], David K. Menon[3,9], and Emmanuel A. Stamatakis[3,4]

[1]Department of Neurosurgery, The Second Affiliated Hospital, Zhejiang University School of Medicine, Hangzhou, China

[2]Frontier Center For Brain Science And Brain-Machine Integration, Zhejiang University, Hangzhou, China

[3]Division of Anaesthesia, University of Cambridge, Cambridge, U.K.

[4]Department of Clinical Neurosciences, University of Cambridge, Cambridge, U.K.

[5]Psychedelics Division - Neuroscape, Department of Neurology, University of California San Francisco, San Francisco, CA, U.S.A.

[6]Centre for Psychedelic Research, Department of Brain Sciences, Imperial College London, London, U.K.

[7]Department of Psychology and Department of Physiology and Pharmacology, Western Institute for Neuroscience, Western University, London, ON, Canada

[8]Trinity College Institute of Neuroscience, School of Psychology, Trinity College Dublin, Dublin, Ireland

[9]Wolfson Brain Imaging Centre, University of Cambridge, Cambridge, U.K.

Abstract

Large-scale functional connectivity (FC) networks are typically treated as discrete neuroanatomical entities, yet their organisation in regions where multiple systems converge remains poorly understood. Here we investigate the posterior precuneus (PCu)—a key hub of the default mode network (DMN) situated at the interface with the frontoparietal control network (FPCN)—using a spatial-derivative approach that quantifies how FC changes along the PCu's dorsal–ventral axis. Across five pharmacological datasets encompassing psychedelic and anaesthetic states, we demonstrate that the spatial derivative of functional connectivity (FC) recovers canonical DMN–FPCN organization with superior anatomical specificity compared to FC alone. This functional gradient is systematically modulated by consciousness level: its overall magnitude diminishes across all altered states of consciousness (ASCs), while its spatial entropy increases under psychedelics but decreases under sedation. These effects cannot be explained by local smoothing and instead suggest that the PCu embeds a continuous, anatomically constrained transition between large-scale networks that is sensitive to global brain-state dynamics. Our findings motivate a gradient-based perspective on functional network organisation and identify a parsimonious neural signature that tracks the brain's dynamical repertoire across diverse ASCs.

Introduction

The search for the neural basis of consciousness has increasingly focused on large-scale brain networks and the ways in which they interact. Over the past two decades, functional neuroimaging studies have shown that whole-brain activity can be described by a set of replicable latent patterns—intrinsic functional connectivity networks (ICNs) [1, 2]. These patterns can be identified using dimensionality-reduction methods such as ICA, PCA, and nonlinear embedding techniques [3], and they correspond reliably to major anatomical features of the cortex. However, this correspondence becomes less clear in regions where multiple systems converge, such as the posteromedial cortex. This area contains mixed cytoarchitecture [4] and shows overlapping signatures from several ICNs [5, 6]. Adding further complexity, functional connectivity patterns dynamically reconfigure over time in response to changing cognitive and physiological demands [7–10].

Despite ongoing debate about the anatomical boundaries of canonical networks [11, 12], the use of network integrity as a biomarker has grown rapidly across neurological and psychiatric research. In these contexts, network integrity is typically evaluated by examining the anatomical regions assumed to constitute each network [13]. Yet the ambiguous properties of certain key brain areas have contributed to inconsistent findings and occasional misinterpretations in the literature. More broadly, clarifying how the functional roles of brain signals relate to their structural substrates remains a central problem for systems neuroscience. While some confusion may stem from measurement noise, preprocessing choices, interpersonal variability, or inconsistent anatomical terminology, these issues also motivate a deeper question: to what extent can ICNs truly be defined or dissociated on the basis of anatomical location alone?

A major source of this uncertainty lies within the posteromedial cortex (PMC)—the central hub of the default mode network (DMN) and one of the least understood regions of the cerebral cortex. Within the PMC, the precuneus (PCu) in particular has a complex functional profile and has often been difficult to delineate clearly [12]. While the posterior cingulate cortex (PCC) is unequivocally a DMN node, the PCu is anatomically a medial extension of the superior parietal lobule (Brodmann Area 7) and frequently coactivates with task-positive regions [14]. This anatomical positioning, together with its relatively high metabolic rate, suggests that the PCu may operate as a convergence zone for integrating information from multiple large-scale systems [15, 16]. The region is also consistently implicated in altered states of consciousness (ASC) [14, 17–19]. Although the

posterior PCu is often considered part of the DMN [10], recent evidence indicates that its anterior portion does not fall cleanly into either the DMN or the FPCN [20]. For clarity, we use PCu in this paper to refer specifically to the posterior precuneus.

The DMN is known for supporting self-generated and internally oriented cognition, and is highly active in the absence of external cues. In contrast, the frontoparietal control network (FPCN) is a core task-positive system, activated during demanding, goal-directed behaviours. Their activity patterns are often anti-correlated during rest, and this balance progressively diminishes with reduced levels of consciousness [21–23]. Understanding how these networks interact is therefore highly relevant to theories of conscious processing [24]. The PCu—situated between them anatomically, metabolically, and functionally—is a natural site in which to probe this interaction.

Building on our previous work demonstrating that differentiation within the precuneus supports cognitive flexibility during tasks [25], we hypothesised that: (1) the dorsal–ventral axis of the posterior PCu contains a functional gradient reflecting a transition between DMN and FPCN connectivity rather than a discrete boundary, and (2) this gradient relates systematically to consciousness level. To test these hypotheses, we analysed multi-site fMRI data across altered states of consciousness induced by both psychedelic and anaesthetic drugs, alongside normal waking state in the same individuals. This combination provides an effective design for sampling a broad spectrum of global brain energy—from heightened to suppressed relative to baseline—and allows us to assess the behavioural relevance of our functional measure. It also enables us to identify system-level alterations common across different forms of ASC, beyond the specific effects of any single drug.

To directly assess how functional differentiation emerges within a convergence zone, we quantified the gradient of functional connectivity relative to the anatomical displacement of seed locations within the PCu. This approach allows us to examine whether the organisation of ICNs within this region follows anatomical boundaries or instead reflects more continuous, gradient-like transitions. Our findings challenge the notion that ICNs can be fully delineated on the basis of anatomy alone, provide new evidence regarding consciousness-specific organisation of functional connectivity in a key region.

Results

The study utilized multisite resting-state fMRI datasets, which included pharmacological interventions in healthy human participants. These datasets were collected by our lab and shared by collaborators. The drugs included Lysergic acid diethylamide (LSD), psilocybin (PSILO), ketamine (KETA), and propofol. Two propofol groups with different sedative effects were used, one from the London Ontario site (PPFL-L) which induced deep sedation, and another from our Cambridge site (PPFL-C) which induced moderate sedation. All datasets similarly employed a within-subject design with randomised fMRI scanning conditions: one involving pharmacological induction of one type of altered state of consciousness and the other involving a placebo (Fig. 1). In total, a hundred healthy participants were involved in this study: n(LSD) = 20, n(PSILO) = 15, n(KETA) = 21, n(PPFL-L) = 19, n(PPFL-C) = 25. All datasets have been referenced in prior publications, with detailed experimental information available in those works. References and key parameters of these experiments are included in the supplementary materials. To minimise cross-centre variability, we conducted preprocessing on the raw data in the exactly same way (see Methods)

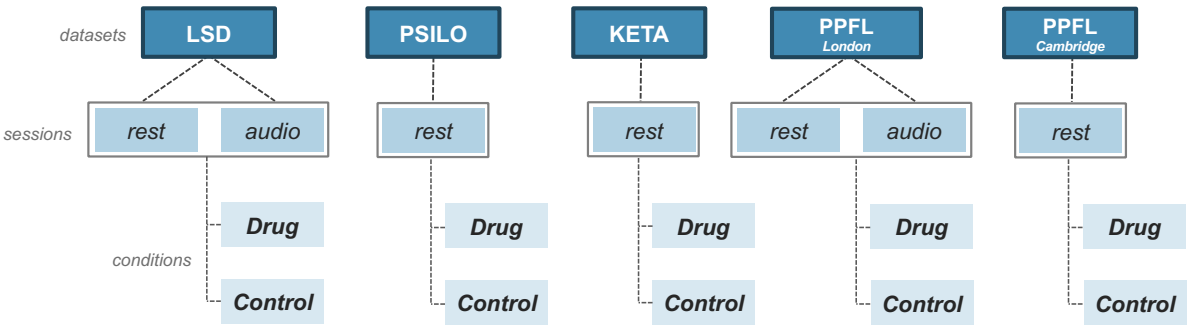


Figure 1: **The structure of datasets used in this study.** Datasets are indicated by the drugs (and sites) involved in the previous studies, which are Lysergic acid diethylamide (LSD), psilocybin (PSILO), ketamine (KETA), propofol from the London Ontario site (PPFL-L) and propofol from the Cambridge site (PPFL-C). In the LSD and PPFL-L datasets, sessions are divided into two types as one of them involved audio stimuli, with music for the LSD study and story narration for the PPFL study. All of the studies have a within-participant design, with drug administration in one of the participant's two visits and placebo administration in another visit.

PCu's FC and its gradient along the dorsal-ventral axis

We first established a baseline for the proposed neural phenomena by confirming their replicability in control groups (i.e., drug-free, awake) across all multi-centre datasets. To examine FC differences relative to the graded spatial displacement along the dorsal-ventral axis of the precuneus, we analysed three precuneal subregions: the dorsal (dPCu) and ventral (vPCu) PCu from a previous study [25] (Fig. 2a), and a new middle PCu (mPCu) situated between them (Fig. 2b). These three adjacent, non-overlapping ROIs provide a linear approximation of continuous sampling along the d-v axis.

As a proof of concept, we examined the seed-based FC of the dPCu, mPCu and vPCu during normal awake conscious states. To do so, we conducted a group-level GLM using the data from control conditions of all datasets, and corrected the main effects of different scanning sessions. As predicted, the resting-state FC (rsFC) of the dPCu, mPCu, and vPCu showed similar positive correlation patterns, primarily covering the default mode network (DMN) (Fig. 2c,d, Fig. S1), in agreement with our previous publication using different datasets [25], and consistent with existing literature depicting the posteromedial cortex as a unified DMN core.

Still in the control condition, we next modelled FC changes against d-v seeding position for all brain voxels, with the slope of this linear model representing the rate of FC change—the precuneal functional gradient (pFG) (i.e., the derivative of FC: $\frac{\Delta \text{FC}}{\Delta \text{displacement}}$). The results supported our hypothesis of a gradual FC transition along the d-v axis (Fig. 2f: Hypothesis 3). Specifically, the positive and negative slopes essentially mirrored the spatial patterns of the DMN and frontoparietal control network (FPCN), respectively, and with greater anatomical specificity: the regions showing stronger gradients are more constrained and focal to the core parts of the networks. The resemblance between the precuneal FC and its spatial derivative provides new information about the brain organisation: the rest of the DMN regions (such as the orbitofrontal cortex, angular gyrus, hippocampus etc.) do not only have strong connectivity with the PCu subregions, but their FC also undergo the fastest changes (i.e. the deepest slopes) along the d-v axis of the PCu.

Since we used a linear model, the result also implies a continuous transition between the DMN and FPCN. As the seed location shifts along the d-v axis, the FC pattern gradually changes from resembling the FPCN to more closely matching the DMN. Quantitatively, positive and negative linear slopes within the DMN and FPCN indicate pro-

gressively stronger and weaker FC with these networks, respectively. While abrupt FC changes often demarcate functional boundaries [26], we demonstrate that precuneal FC exhibits continuous transitions along its d-v axis—an anatomical trajectory bridging the FPCN and DMN. These findings suggest that the DMN and FPCN may be inseparable systems, anchored by the PCu's structural organisation (Fig. 2f: Hypothesis 4).

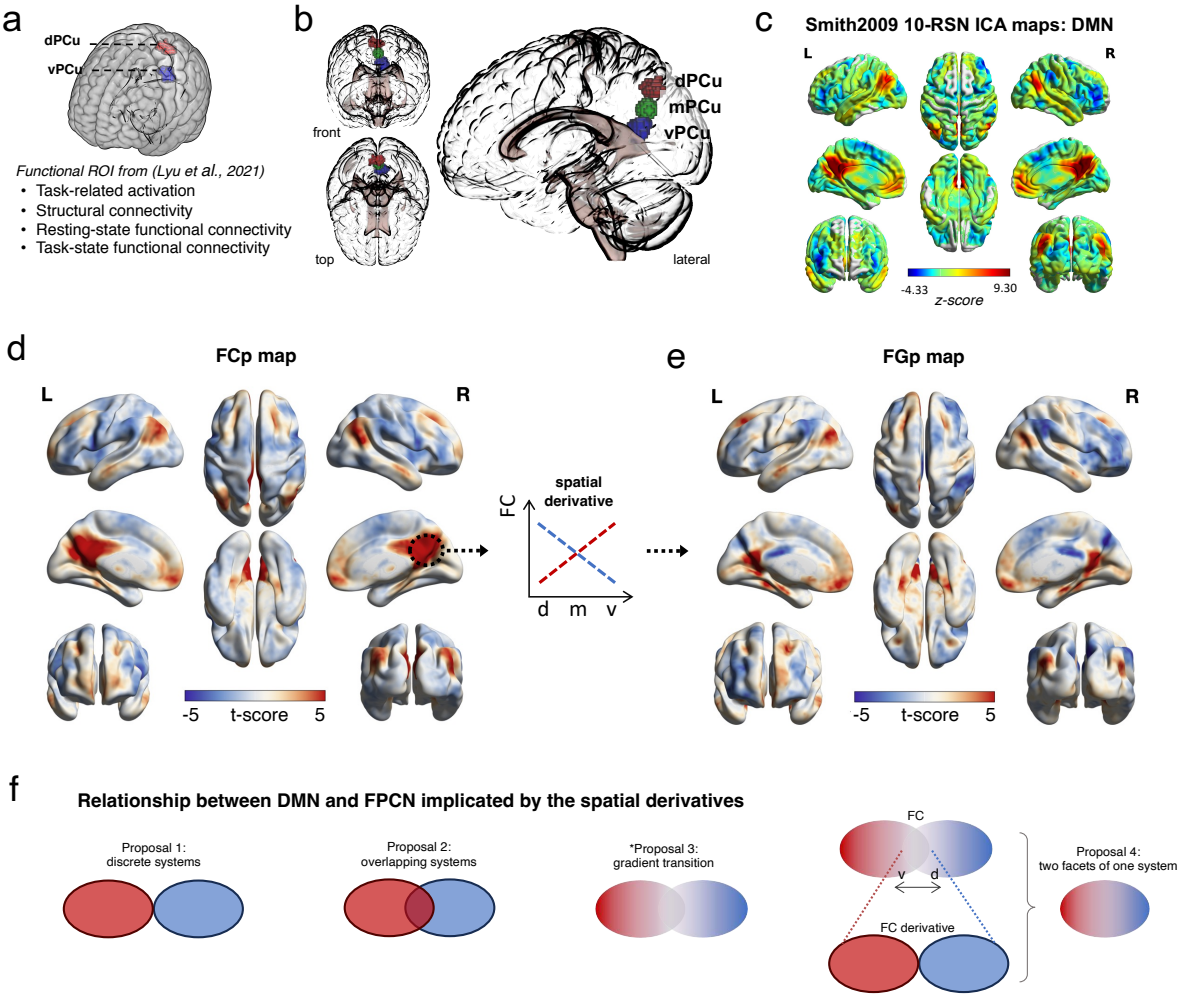


Figure 2: **Spatial derivative of the precuneual FC, i.e., functional gradient of the PCu (FGp)** (a) Derivation of d/vPCu from our previous publication [25]. (b) Visualisation of d/m/vPCu in a 3-D standardised brain from the front, top and lateral perspectives. The mPCu is taken as a spherical (radius = 6.5 mm) ROI midway between the dPCu and vPCu. (c) A canonical spatial map of the DMN (from *Smith2009* 10-RNS atlas [27]). (d) A seed-based PCu FC unthresholded spatial map generated with the multisite datasets for the control condition (adjusted for the main effects of different scanning sessions), averaged across the d/m/vPCu seeds. Group-level t-scores are presented, indicating the main effect of the voxel-wise correlation strength, computed with a standard mixed-design general linear model (GLM) approach (see Methods). Warm colour indicate positive FC and cold colours indicate negative FC. (e) Unthresholded FGp spatial map, generated with a linear regression using the relative location of the subregions as a independent variable (x-axis) and each subregion's FC as a dependent variable (y-axis), computed on whole-brain voxels. Presented are group-level t-scores of the FGp strength (i.e., how deep the slope was). Warm colours indicate positive slopes (i.e., increasing FC along the d-v axis) and cold colours indicate negative slopes. (f) Relationship between DMN and FPCN implicated by the self-similar pattern of spatial derivatives. Proposal 1&2 are common assumptions in the literature. Our study was motivated by our initial hypothesis (Proposal 3) that the DMN and FPCN has gradient transitions as these large-scale networks have a probabilistic entity. However, the observed self-similar patterns between the precuneal FC and its spatial derivative indicates a more radical hypothesis (Proposal 4): the DMN and FPCN may be considered as a unified system with inherent spatial continuity.

Diminished FGp during altered states of consciousness

We further asked whether the FGp is functionally relevant; in other words, whether and how it is changed in altered conscious states (Fig. 3a). As we previously identified FGp to be mainly localised in the DMN and FPCN, we adopted the Regions Of Interest approach by using network masks to constrain data extraction for further comparisons. In addition, we found group-specific data-driven network discovery (i.e. Independent Component Analysis/ICA) approach provided more precise network overlay with the FGp maps than predefined networks (i.e., Yeo2011-7Net or Smith2009-10RSN); therefore, we used the ICA network masks for the subsequent analyses (Fig. 3b). Specifically, denoised control-group data were fed into ICA and dual-regression for each dataset, respectively (Fig. S2-S6). Boundary cutoff was set to be 3 or 4 z-score to achieve an ideal known pattern of the network for each dataset .

FGp magnitudes were shown to diminish in the drug conditions comparing to the control condition within each dataset. Significant clusters of the FGp for each dataset were presented in Fig. 3c, with the red clusters corresponding to positive FGp (i.e., in the d-v direction), and blue clusters corresponding to negative FGp (in the v-d direction). To formally test the diminished size of the significant FGp clusters, we contrasted the group-level FGp (i.e., the values of each voxel in the DMN and FPCN mask) between the drug and control conditions. By doing so, the statistical inference was made at the network level rather than voxel level. Permutation tests (n = 100,000) were conducted against the null hypothesis (i.e., zero difference between conditions), with the one-tailed test. Family-wise error were controlled with Bonferroni procedure of Holm for the multiple comparisons for all the datasets and FC types (including unthresholded FC and the FC separating positive and negative correlations, which generating similar results; the main figures were based on the unthresholded FC) (see S1).

As hypothesised, during ASC under the drug effect, regardless of the drug type, the distribution of FGp in the DMN mask shifted leftwards (i.e., became less positive); while the distribution of FGp in the FPCN mask shifted rightwards (i.e., became less negative), compared to the control condition (Fig. 3c, Supplementary Table S1). As the FGp is derived from a linear trend of differences across the d/m/vPCu's seed-based FC, this result indicates that during a normal conscious state, there is a stronger stretch of FC differentiation across the d/m/vPCu, while the FC differentiation is flattened as consciousness is altered by drugs.

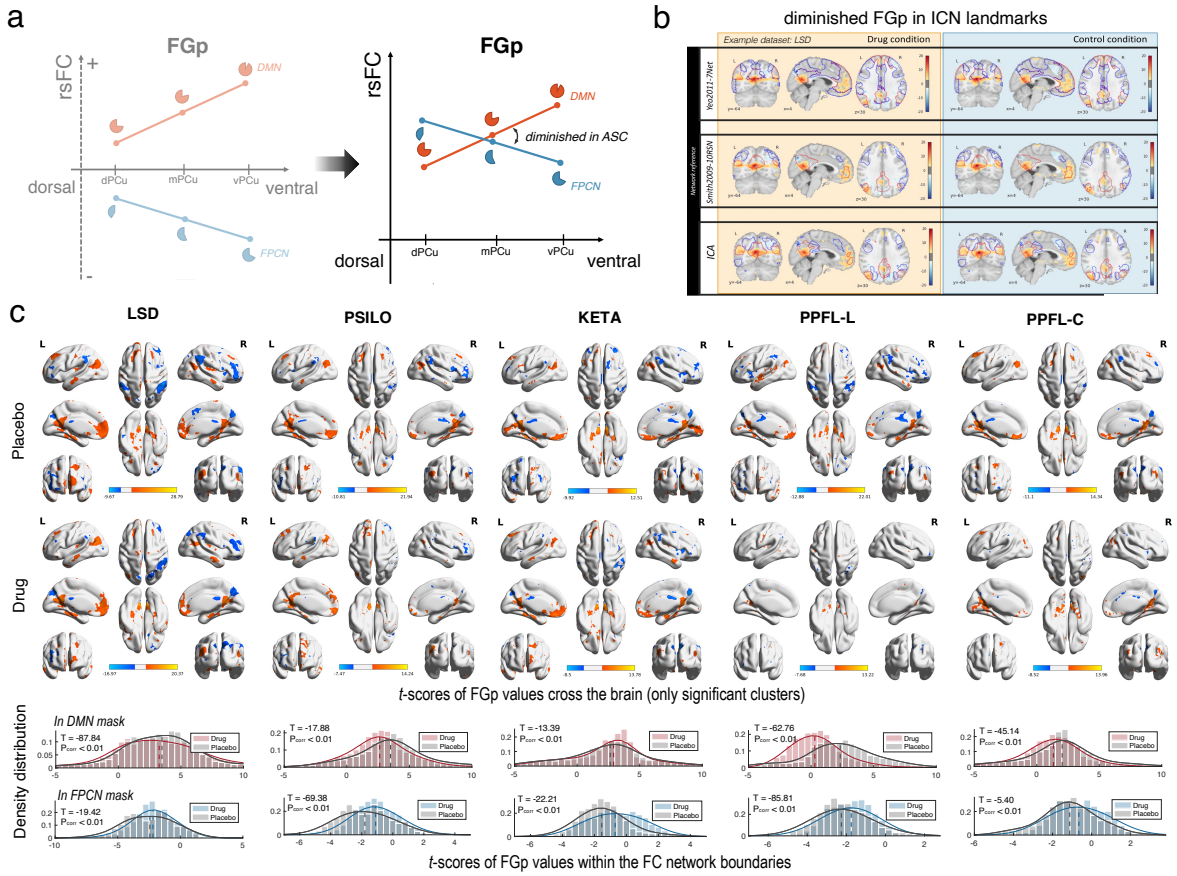


Figure 3: **Functional relevance of FGp indicated by its impairment during ASCs** (a) Hypothesised statistical model of FGp during altered states of consciousness (ASC). (b) Example of significant FGp clusters in cross-sectional brain views (i.e., the brain heatmap), superimposed with multiple spatial references of the intrinsic connectivity networks (ICN) (coloured contours, red: DMN, blue: FPCN), compared between drug (left) and control (right) conditions. The presented dataset is LSD. The spatial references of the ICNs includes published atlases: Yeo2011-7net [28], Smith2009-10RSN [27], and the network discovery with independent component (IC) analysis on the present control condition of each dataset. (c) Significance clusters of FGp in surface views, compared between normal awake condition and the experimental condition of altered states of consciousness induced by different drugs: lysergic acid diethylamide (LSD), psilocybin (PSILO), ketamin (KETA), propofol (PPFL). Two PPFL datasets were used respectively from London (-L) and Cambridge (-C) study sites (see Methods for details). Each column panel represents the set of FGp results for each dataset. For each set of results, presented are the FGp maps (thresholded with significance testing of cluster-wise $P_{FWE-corr} < 0.05$) in both control (top row) and ASC (middle row) conditions, below which are the histograms of the unthresholded FGp scores (normalised with t-scores) within either DMN or FPCN network boundaries. Network boundaries were identified based on the thresholded (z-score > 3) independent component maps generated from the corresponding cohort during a normal conscious condition.

Drug-specific effects on the spatial entropy of FGp

With the previous analyses, we have showed a common profile of diminished FGp during ASC states, regardless of the differences in the experiential contents that are associated

with the drugs. However, psychedelic and sedative drugs have distinct effects on mental states, which have been situated at the opposite ends of a normal waking conscious state [29]. We asked whether the FGp is also relevant to the general type of conscious states as it may differ among drug-specific effects. We examined the spatial entropy (Fig. S7), i.e., how "chaotic" or "unpredictably" the functional gradient of the PCu is distributed within the DMN and FPCN masks, across different datasets. According to the Entropic Brain Theory (EBT), normal waking consciousness is situated at a closely critical (albeit slightly sub-critical) state, which could be shifted into a more disordered and flexible state by psychedelic drugs, or switched to a more predictable and stereotypical state under sedation [29].

Consistent with our previous analysis, the averaged FGp within networks showed a similar pattern across different drugs, as the interaction effect was not significant between datasets and conditions, meanwhile the drug-induced main effect showed opposite patterns between the DMN and FPCN ($\Delta = -0.02, p_{adj.} = 0.04$ for DMN, $\Delta = 0.005, p_{adj.} = 0.40$ for FPCN) (Fig. a).

On the other hand, the spatial entropy of the FGp was shown to vary across different drugs, as the interaction between datasets and condition was significant for both networks ($Chisq = 35.71, p = 0.00$ for DMN; $Chisq = 10.56, p = 0.03$ for FPCN). Although the post-hoc pair-wise tests were not all significant, the main effects of different drugs showed hypothesised directions: the psychedelic drugs tend to increase the spatial entropy of the FGp, i.e. making the spatial distribution of the FGp within networks more diverse ($\Delta = 0.02, 0.02$, respectively for LSD in FPCN and for PSILO in DMN); while the sedative drugs tend to decrease that, i.e. making the spatial pattern more uniform ($\Delta = -0.38, -0.18, p_{adj.} = 0.00, 0.045$ respectively in DMN & FPCN for PPFL-L , and $\Delta = -0.02, -0.03$, in DMN & FPCN for PPFL-C).

We further combined the metrics between the networks to show a general pattern of the drug-induced changes. We took (1) the difference between DMN and FPCN for the mean of FGp, and (2) the sum of the their spatial entropy, as combined network measures, and compared their drug-induced changes across different types of ASC (with z-scores of their pair-wise changes). Consistent with intra-network statistics, we showed that the inter-network gradients were generally diminished in all kinds of altered states of consciousness, but the spatial entropy of the gradients varied, with the psychedelic drugs generally showing a increased trend ($t = 1.91, 2.90, p_{adj.} = 0.08, 0.01$ for LSD and KETA) and the anaesthetic drugs showing a decreased trend ($t = -6.82, -1.70, p_{adj.} = 0.00, 0.12$

for PPFL-L and PPFL-C). In addition, we notice that the effect sizes of the altered FGp and spatial entropy correspond to the relative drug dosages that are varied among these datasets.

The results are in line with previous studies on the spatial domain which found Shannon entropy of the degree distribution of networks was increased during Ayahuasca-induced ASC [30] and decreased during propofol-induced ASC [31]. However, it should also be noted that the distinct drug effects on the entropic measure in our study were not robustly consistent across different datasets of the same drug type, as the PSILO dataset showed a significant opposite pattern to the one hypothesised. This may be caused by dosage differences or other confounding factors. More independent datasets would be needed here to make strong arguments about the EBT.

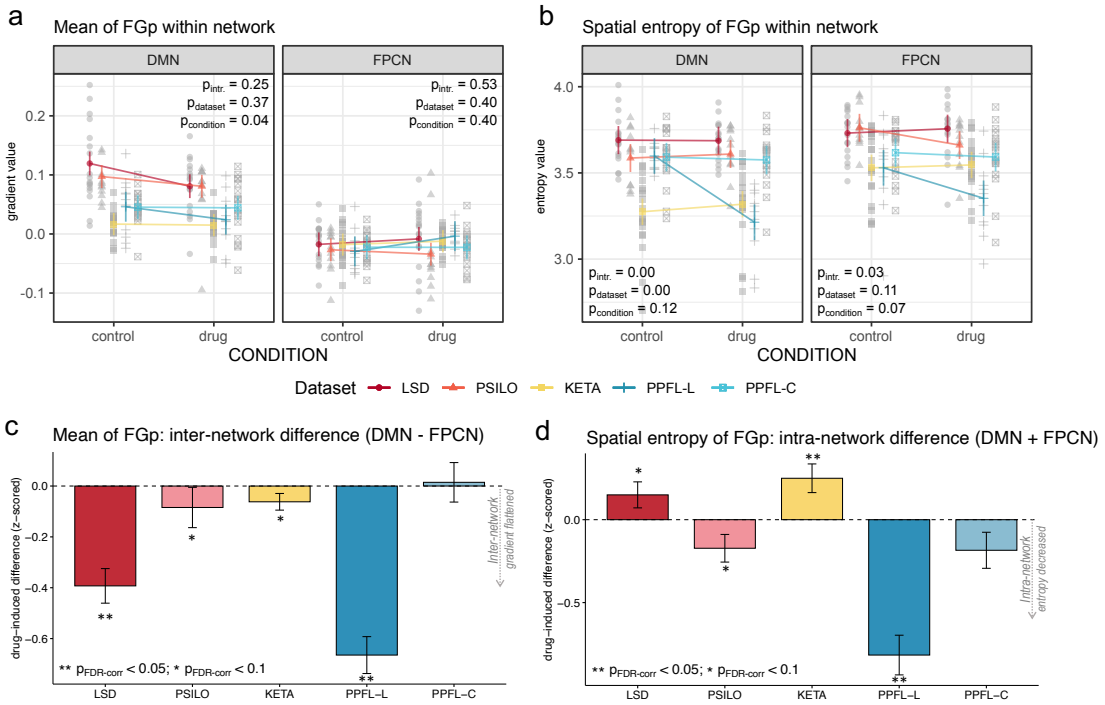


Figure 4: **The mean and spatial entropy of the precuneal functional gradient (FGp) altered by different drugs** (a) and (b) respectively show the mean and spatial entropy (H) of the FGp within the DMN and FPCN masks and how the drug-induced effects (compared to its own control condition) are differed or similar across different drugs/datasets. A short summary of statistics were provided, with the $p_{intr.}$, $p_{dataset}$ and $p_{condition}$ respectively indicating the significance of the interaction effect between drug types and conditions, and their own main effects. Notably, the main effect of datasets is calculated based on its effect on the pair-wise comparisons between control and drug conditions. All the reported significance thresholds have been adjusted with false-discovery-rate (FDR) correction for multiple comparisons. (c) and (d) showed drug-induced differences with combined network effect, respectively for the mean of FGp and the spatial entropy of FGp. The functional gradients altered in opposite directions for DMN and FPCN in the drug condition, hence the combined network effect took the difference of the drug-induced changes (noted as "DMN-FPCN"), which amounts to the narrowed angle between the two slopes illustrated in Fig. 3c. The altered spatial entropy of FGp in the drug conditions showed similar patterns between DMN and FPCN, hence the combined network effect took the summary of their scores (noted as "DMN+FPCN"). The drug-induced difference was z-scored against the standard deviation of each dataset's placebo condition. The error bars indicated standard error.

Discussion

In this study, we examined how functional connectivity (FC) varies relative to the anatomical organisation of the posterior precuneus (PCu). We found that the dorsal–ventral (d–v) axis provides a principled anatomical scaffold that differentiates the default mode network (DMN) from the frontoparietal control network (FPCN): the relative FC differences (i.e., the gradient) along the d-v axis revealed these two networks, and with higher anatomical specificity than the FC patterns itself. Importantly, the PCu's functional gradient was also systematically modulated across altered states of consciousness (ASC). While ASCs reduced overall gradient magnitude, psychedelics and sedatives produced opposite effects on spatial entropy of the PCu's gradient: psychedelics increased entropy, whereas anaesthetics decreased it. These indicate that the PCu gradient alone captures key changes of the brain's dynamical repertoire across conscious states, a finding previously shown to emerge at the level of network interactions [32–35].

Taken together, these findings have implications for how large-scale functional connectivity (FC) networks are defined and interpreted. Although contemporary neuroimaging continues to advance toward increasingly fine-grained cortical parcellations, FC networks arise from different principles, and their underlying neural mechanisms remain incompletely understood. They should therefore not be treated as equivalent to parcellation schemes grounded in clear physical or anatomical features. As any parcellation scheme implicitly reflects a model of how one believes the brain is organised [36], we instead view functional networks as dynamic equilibria emerging from ongoing interactions among distributed neural populations, for which sharp boundaries may not exist. With the presented results, we hope to elucidate this point by focusing on the well-known case of DMN-FPCN interactions, and we found at a local scale, how the dorsal PCu systematically connects with the whole brain underlies the DMN-FPCN separation. The continuous transition we observe within the PCu also highlights how network boundaries may reflect gradual changes in anatomical embedding rather than discrete partitions.

This perspective offers clinical implications. Using spatial patterns of large-scale networks as biomarkers can be problematic when atrophy or structural reorganisation is present. However, network alterations may reflect shifts in the broader energy landscape of whole-brain dynamics, which is a phenomena that can be captured independently of the networks' spatial configurations. This view also carries theoretical implications for understanding information integration in the brain. The traditional contrast between the

DMN as supporting "internal" processes and the FPCN as supporting "external" ones may be overly rigid. Although conceptually distinct, these dimensions of conscious experience are tightly intertwined in practice, and recognising their graded relationship may help avoid theoretical challenges that arise when they are treated as functionally opposed systems.

Our results suggest that alterations in PCu function during altered states of consciousness may underlie the observed breakdown of network interactions. Recent rodent work has shown that ketamine-induced dissociation-like behaviour is associated with a low-frequency oscillation in the homologous region of human PMC (but rodents may not have finer functional specialisation of PMC subregions), and that optogenetic stimulation in this area can reproduce the behaviour [17]. In human neuroimaging studies using pharmacologically induced ASCs or clinical cohorts with reduced consciousness, the integrity of the DMN FC and its anticorrelations is often particularly sensitive [23, 32, 34, 37]. Our findings suggest that this network-level effect may be more parsimoniously explained by altered function of the PCu. The spatial derivatives of PCu FC recovered canonical DMN–FPCN organisation with greater anatomical specificity and showed similar—if not better—sensitivity to different conscious states. Since the gradient captures *changes* in FC rather than shared similarity, these effects cannot be attributed solely to local smoothing. Instead, they suggest that the organisation of whole-brain activity is richly structured across both space and time. This interpretation aligns with the studies showing that dynamic FC on short timescales recapitulates the spatial organisation and behavioural relevance of static FC [30, 38]. Together, these findings suggest that global cortical activity has a multidimensional and complex origin, of which FC networks derived from signal correlations represent only one observable facet.

Although this view departs from classical models that treat FC networks as clusters of cortical areas with distinct microstructural profiles [26, 39], we recognise that functional networks do have structural underpinnings. Previous studies have attributed the DMN construction to diffusion tensor imaging (DTI)-based structural connectivity (SC) of its subregions [40, 41], though SC and FC do not correspond in a one-to-one manner [42]. Among the subregions, the PCu was shown to have gradient SC along its dorsal-ventral axis in the previous literature. Structural connectivity with virus tracing in macaque brains showed that the more ventral regions in the PMC (BA homologous 23 and 31) are more reciprocally connected to frontal areas such as the frontal pole and ACC, while the dorsal PCu (7m) selectively connects with the back of the brain such as parietal and

occipital cortices but lacks connections with the vmPFC/ACC [43, 44]. Similarly, human evidence from DTI also showed that from dorsal to ventral parts of the PCu, there is a spectrum of increasing connectivity with DMN regions (such as the hippocampus and mPFC) and decreasing connectivity with sensorimotor, visual networks, thalamus, and cognitive control regions (such as AnG, SPL, prefrontal and premotor areas) [25, 41, 45]. These anatomical gradients may therefore support the functional gradient reported here.

Beyond cortico–cortical pathways, subcortical structure may also shape the PCu's gradient. Tracer evidence in macaques demonstrates topographic projections from PMC to distinct zones of the dorsal thalamus [43, 46]. Given the extensive PMC–thalamus connectivity [10, 45], disruptions in thalamocortical gating have been proposed as a common mechanism for various ASCs [47, 48]. Correspondingly, altered thalamus–DMN coupling has been observed across epilepsy, anaesthesia, and pharmacological manipulations [49–51]. Linking PCu gradients to thalamocortical pathways will therefore be an important direction for future research.

Several limitations warrant consideration. First, our study is aimed to find commonality of brain mechanisms for a spectrum of altered states of consciousness. Although we found differential spatial entropy of pFG that roughly corresponds to the intended directions, we only had two datasets for each of the two ends of the spectrum (sedation versus psychledic), which did not provide sufficient evidence to claim that the spatial entropy of pFG reflects the quality of ASCs. Second, although we focused on the posterior PCu, similar continuous transitions may exist elsewhere, such as within the PCC [52] and the posterior parietal cortex [53]. Third, our GLM relied on three regions of interest; datasets with higher signal-to-noise may allow finer-grained sampling along the d–v axis, where we expect the overall pattern to remain robust. Finally, not all functional boundaries may be gradient-like: for example, the interface between posterior and anterior PCu appears relatively sharp, corresponding to proposed distinctions between the DMN and the "action mode network" [54]. Thus, gradient-based and boundary-based organising principles likely coexist across cortex. Future studies should therefore tailor anatomical hypotheses to specific regions and scales of organisation.

Methods

Preprocessing

All of the preprocessing steps were carried out with the toolbox SPM12 (`https://www.fil.ion.ucl.ac.uk/spm/software/spm12/`) based on the Matlab platform. In order to maximise the precision of our functional mapping of the multi-site datasets, we conducted all the statistics in the individual space, and only sorted to a normalised space when a group-level inference was needed. Therefore, the preprocessing steps have a slightly different order than a default fMRI image processing pipeline. Specifically, the data was minimally preprocessed before the step of normalisation, which included the standard steps including structural image tissue segmentation, skull stripping, functional image realignment, motion scrub, and co-registration to the individual skull-stripped T1 image. The normalisation was performed with the DARTEL toolbox non-linear algorithm (`https://www.fil.ion.ucl.ac.uk/spm/ext/`) and it was conducted after individual-level statistics were obtained.

For motion detection and correcting for motion-induced artefacts, we used the *ArtRepair* toolbox (`https://cibsr.stanford.edu/tools/human-brain-project/artrepair-software.html`). Scanning sessions with more than 20% of the volumes corrupted were excluded for further analyses. As a result, the data of 2, 3, 1, 6, 8 participants have been excluded respectively from the datasets LSD, PSILO, KETA, PPFL-L and PPFL-C.

Non-neuronal nuisance signals were extracted with the Component Based Noise Correction method using anatomical masking (aCompCor), and were used as covariates in the subsequent general linear models.

Data analysis

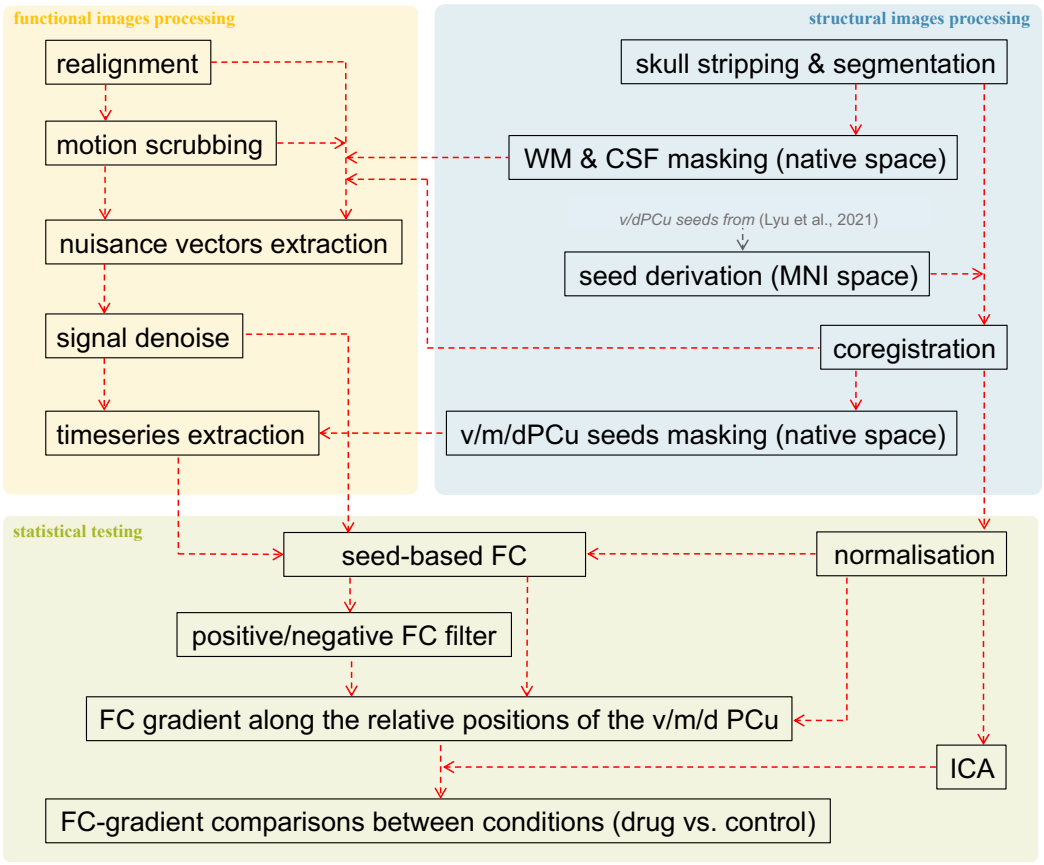


Figure 5: **Illustration of the data analysis pipeline.**

ROI analyses

The d/vPCu seeds were adopted from the previous project. Since they were functional ROIs derived from task-associated (de)activations, they do not have a shape as regular as the spherical seed mPCu; but the volume of the d/vPCu is comparable to the mPCu. We used the canonical ICNs as landmarks to reference the d/m/vPCu' spatial localisation. Specifically, we adopted two network atlases, one thresholded (*Yeo2011* 7-network atlas) and one unthresholded (*Smith2009* 10-RSN atlas) [27, 28] (Fig. SS1).

The ROIs were identified first in the standard space, then transformed to the native space for signal extraction. Specifically, ROI masks are represented by binary values signifying which voxels to extract values from, and the first eigenvalue from the voxels (after removing the nuisance signals) were extracted. The ROIs were manually checked to ascertain they were correctly co-registered to the native space.

The dorsal and ventral precuneus ROIs were obtained from our previous study [25]. To examine the functional gradient along the dorsal to ventral axis in the precunues,

we derived the middle point between our previously published two ROIs. To ensure the d/vPCu and the middle PCu (mPCu) have about the same cluster size, we used the radius of 6.5 mm for making the mPCu (sphere-shaped) ROI. We also excluded voxels that overlapped between the ROIs. As a result, the cluster sizes for the d/m/vPCu are respectively 150, 135, 168 (voxels), aligned along the d-v axis of the precuneus. The above procedures were conducted using the *FSL* utilities (`https://fsl.fmrib.ox.ac.uk/fsl/fslwiki/Fslutils`).

Independent component analysis (ICA)

The Probabilistic Independent Component Analyses (ICA) were carried out independently for each dataset and only on the control condition (normal conscious state) in order to derive the group-specific functional networks, which is used as an alternative to standard network atlases. It was conducted with the MELODIC toolbox (Multivariate Exploratory Linear Decomposition into Independent Components) Version 3.14, in *FSL* (FMRIB's Software Library, `www.fmrib.ox.ac.uk/fsl`). Data from all participants of each site were concatenated together for conducting the group-level ICA. The resulting components can be identified as the canonical ICNs for that group. The ICA efficacy for separating the data into conventionally defined ICNs has been manually checked. In line with the previous literature [27], 30 components were designated for the algorithm to separate from the data, and generated good results, except for the the PPFL-C dataset on which we finally specified 40 components to ensure a good separation of the FPCN from other task-positive networks. The resulting DMN and FPCN IC components for each dataset have been presented in Supplementary Figures S2-S6 For deriving the network masks for timeseries extractions, the IC images indicating the DMN and FPCN were threshold with $Z = 3$ and binarised for all datasets.

Seed-based Functional Connectivity (FC) and functional gradient of the PCu (FGp)

For seed-based FC, a GLM was conducted for each seed, with the main regressor being the time-series of the seed signal, as well as the covariates of the 6 movement regressors and the 14 nuisance vectors which were the non-neuronal components extracted from the WM and CSF. For the datasets (LSD, PSILO and PPFL-L) that have multiple sessions for each subject, this GLM was extended with different sessions modelled as different

blocks and the confounding covariate included the global session effect. The correlation coefficient associated with the time-series of the seed was taken as the FC, which was estimated for all brain voxels. For the group level analysis, the coefficient maps in the native space were normalised and grouped together for further analyses. Acknowledging the fact that the positive and negative FC may have different characteristics, we also separated the coefficient maps at the individual level into positive and negative ones for further analyses. For the PCu gradient analysis, the d/m/vPCu's relative positions on the d-v axis were assigned to a linear vector of -1, 0, 1, and used the independent variable. The FC maps of the d/m/v PCu output from the previous step were used as the dependent variable. The beta associate to the linear vector of the d-v axis in this GLM is a gradient map indicating how the FC linearly varies (i.e. the slope) along the d-v axis of the PCu.

The group-level inferences were conducted independently for each dataset, using one-sample T tests for the baseline seed-based FC maps and the gradient maps (FGp) of the PCu's FC. To compare how the gradient maps vary between conditions, we subtracted the gradient maps between the placebo and the drug conditions, and did permutation tests on the contrasted gradient maps within network masks. Overlaps between the DMN and FPCN, and between the network and seed (d/m/vPCu) masks, were excluded from the network masks. By a visual examination, the group-level gradient maps in the drug conditions appeared to be less prominent than those in the placebo conditions; therefore, in the presented statistical testing, only one-tailed tests were used; i.e., to determine whether the gradients in the drug condition are significantly lower than those in the placebo condition.

Shannon entropy, statistical testing and multiple comparison correction

The measure of spatial entropy was meant to capture how variable the values are spread within certain area. To do this, Shannon entropy was calculated on the FGp and FC distributions among the voxels within network masks: $H(X) = -\sum_{i=1}^{n} P(x_i) \ln P(x_i)$, with X being a distribution of voxel values, n being the total number of bins for the distribution, x_i being the i^{th} range/bin, and $P(x_i)$ being the probability of a voxel value falling in the range of x_i. To decide what bin number to use for calculating H, a function of H against bin numbers was made from group-averaged FGp and analysed. As a result, a bin number of 100 was used because according to H's first and second derivatives over the

bin number, this is when H reaches a stable natural logarithmic increase as the bin number keeps increasing (see Supplementary Fig. S8). As a sanity check, other bin numbers (12 and 500) were also used as alternatives for the subsequent analyses. The fact that they yielded consistent patterns of group comparisons suggests that the presented entropy result is not contingent on the bin number of 100 chosen (Fig. S9). For delineating the relationships between datasets and drug effect, subsequent statistics included three-way interactions between "Condition", "Dataset" and "Network", two-way interactions between Condition and Dataset for each network (DMN or FPCN), and a series of main effect analyses and post-hoc pair-wise comparisons. Given the non-normal distribution of the data, all of these statistical models were implemented with non-parametric inferences. Significance inferences for nested statistics using the same data were FDR-corrected for multiple comparisons.

Acknowledgement

The authors appreciate support for the research of this work from Wellcome Trust Research Training Fellowship (grant no. 083660/Z/07/Z), Raymond and Beverly Sackler Studentship, and the Cambridge Commonwealth Trust (to R.A.); Canadian Institute for Advanced Research (CIFAR; grant RCZB/072 RG93193) (to D.K.M., A.M.O. and E.A.S.); Cambridge Biomedical Research Centre and NIHR Senior Investigator Awards and the British Oxygen Professorship of the Royal College of Anaesthetists (to D.K.M.); Stephen Erskine Fellowship at Queens' College, Cambridge (to E.A.S.); Canada Excellence Research Chairs program (215063) (to A.M.O.); L'Oreal-Unesco for Women in Science Excellence Research Fellowship (to L.N.); Imperial College President's Scholarship (to L.R.); Alex Mosley Charitable Trust and supporters of the Centre for Psychedelic Research, Ralph Metzner Distinguished Professorship at UCSF (to R.L.C.-H.); Beckley Foundation and Beckley Foundation–Imperial College research program; Patrick Vernon donation mediated by the Beckley Foundation.; British public service broadcast station Channel 4; Neuropsychoanalysis Foundation; Multidisplinary Association for Psychedelic Studies; Heffter Research Institute; Bernard Wolfe Health Neuroscience Fund; Wellcome Trust; Engineering and Physical Sciences Research Council (capital grant EP/T022159/1) and Medical Research Council research infrastructure award (MR/M009041/1).

Data Availability

Raw data were generated from the previous published studies as referenced and shared by our collaborators. Derived data supporting the findings of this study are available from the corresponding author on request.

References

1. Fox, M. D. & Raichle, M. E. Spontaneous Fluctuations in Brain Activity Observed with Functional Magnetic Resonance Imaging. *Nature Reviews. Neuroscience* **8,** 700–711 (Sept. 2007).

2. Cole, M. W. *et al.* Activity Flow over Resting-State Networks Shapes Cognitive Task Activations. *Nature Neuroscience* **19,** 1718–1726 (Dec. 2016).

3. Margulies, D. S. *et al.* Situating the Default-Mode Network along a Principal Gradient of Macroscale Cortical Organization. *Proceedings of the National Academy of Sciences* **113,** 12574–12579 (Jan. 2016).

4. Cavanna, A. E. & Trimble, M. R. The Precuneus: A Review of Its Functional Anatomy and Behavioural Correlates. *Brain* **129,** 564–583 (Mar. 2006).

5. Braga, R. M. *et al.* Echoes of the Brain within Default Mode, Association, and Heteromodal Cortices. *The Journal of Neuroscience: The Official Journal of the Society for Neuroscience* **33,** 14031–14039 (Aug. 2013).

6. Braga, R. M. *et al.* Parallel Distributed Networks Resolved at High Resolution Reveal Close Juxtaposition of Distinct Regions. *bioRxiv,* 475806 (Nov. 2018).

7. Dixon, M. L. *et al.* Interactions between the Default Network and Dorsal Attention Network Vary across Default Subsystems, Time, and Cognitive States. *NeuroImage* **147,** 632–649 (Feb. 2017).

8. Vatansever, D. *et al.* Default Mode Dynamics for Global Functional Integration. *The Journal of Neuroscience: The Official Journal of the Society for Neuroscience* **35,** 15254–15262 (Nov. 2015).

9. Li, R. *et al.* Developmental Maturation of the Precuneus as a Functional Core of the Default Mode Network. *Journal of Cognitive Neuroscience* **31,** 1506–1519 (Oct. 2019).

10. Utevsky, A. V. *et al.* Precuneus Is a Functional Core of the Default-Mode Network. *The Journal of Neuroscience* **34,** 932–940 (Jan. 2014).

11. Uddin, L. Q. *et al.* Towards a Universal Taxonomy of Macro-scale Functional Human Brain Networks. *Brain Topography* **32,** 926–942 (Nov. 2019).

12. Foster, B. L. *et al.* A Tripartite View of the Posterior Cingulate Cortex. *Nature reviews. Neuroscience* **24,** 173–189 (Mar. 2023).

13. Mohan, A. *et al.* The Significance of the Default Mode Network (DMN) in Neurological and Neuropsychiatric Disorders: A Review. *The Yale Journal of Biology and Medicine* **89,** 49–57 (Mar. 2016).

14. Cavanna, A. E. The Precuneus and Consciousness. *CNS Spectrums* **12,** 545–552 (July 2007).

15. Hagmann, P. *et al.* Mapping the Structural Core of Human Cerebral Cortex. *PLOS Biology* **6,** e159 (July 2008).

16. Raichle, M. E. & Snyder, A. Z. A Default Mode of Brain Function: A Brief History of an Evolving Idea. *NeuroImage* **37,** 1083–1090, discussion 1097–1099 (Oct. 2007).

17. Vesuna, S. *et al.* Deep Posteromedial Cortical Rhythm in Dissociation. *Nature* **586,** 87–94 (Oct. 2020).

18. dos Santos, R. G. *et al.* Classical Hallucinogens and Neuroimaging: A Systematic Review of Human Studies: Hallucinogens and Neuroimaging. *Neuroscience & Biobehavioral Reviews* **71,** 715–728 (Dec. 2016).

19. Winkelman, M. J. The Mechanisms of Psychedelic Visionary Experiences: Hypotheses from Evolutionary Psychology. *Frontiers in Neuroscience* **11,** 539 (2017).

20. Lyu, D. *et al.* Causal Evidence for the Processing of Bodily Self in the Anterior Precuneus. *Neuron* (June 2023).

21. Weissman, D. H. *et al.* The Neural Bases of Momentary Lapses in Attention. *Nature Neuroscience* **9,** 971–978 (July 2006).

22. Fox, M. D. *et al.* The Human Brain Is Intrinsically Organized into Dynamic, Anticorrelated Functional Networks. *Proceedings of the National Academy of Sciences of the United States of America* **102,** 9673–9678 (May 2005).

23. Perri, C. D. *et al.* Neural Correlates of Consciousness in Patients Who Have Emerged from a Minimally Conscious State: A Cross-Sectional Multimodal Imaging Study. *The Lancet Neurology* **15,** 830–842 (July 2016).

24. Mashour, G. A. *et al.* Conscious Processing and the Global Neuronal Workspace Hypothesis. *Neuron* **105,** 776–798 (Mar. 2020).

529 25. Lyu, D. *et al.* A Precuneal Causal Loop Mediates External and Internal Information
530 Integration in the Human Brain. *Journal of Neuroscience* (Oct. 2021).

531 26. Glasser, M. F. *et al.* A Multi-Modal Parcellation of Human Cerebral Cortex. *Nature*
532 **536,** 171–178 (Aug. 2016).

533 27. Smith, S. M. *et al.* Correspondence of the Brain's Functional Architecture during
534 Activation and Rest. *Proceedings of the National Academy of Sciences of the United*
535 *States of America* **106,** 13040–13045 (Aug. 2009).

536 28. Thomas Yeo, B. T. *et al.* The Organization of the Human Cerebral Cortex Estimated
537 by Intrinsic Functional Connectivity. *Journal of Neurophysiology* **106,** 1125–1165
538 (Sept. 2011).

539 29. Carhart-Harris, R. L. & Friston, K. J. REBUS and the Anarchic Brain: Toward a
540 Unified Model of the Brain Action of Psychedelics. *Pharmacological Reviews* **71,**
541 316–344 (July 2019).

542 30. Vidaurre, D. *et al.* Brain Network Dynamics Are Hierarchically Organized in Time.
543 *Proceedings of the National Academy of Sciences* **114,** 12827–12832 (Nov. 2017).

544 31. Pappas, I. *et al.* Brain Network Disintegration during Sedation Is Mediated by the
545 Complexity of Sparsely Connected Regions. *NeuroImage* **186,** 221–233 (Feb. 2019).

546 32. Carhart-Harris, R. L. *et al.* Functional Connectivity Measures after Psilocybin In-
547 form a Novel Hypothesis of Early Psychosis. *Schizophrenia Bulletin* **39,** 1343–1351
548 (Nov. 2013).

549 33. Smigielski, L. *et al.* Psilocybin-Assisted Mindfulness Training Modulates Self-Consciousness
550 and Brain Default Mode Network Connectivity with Lasting Effects. *NeuroImage*
551 **196,** 207–215 (Jan. 2019).

552 34. Threlkeld, Z. D. *et al.* Functional Networks Reemerge during Recovery of Conscious-
553 ness after Acute Severe Traumatic Brain Injury. *Cortex; a Journal Devoted to the*
554 *Study of the Nervous System and Behavior* **106,** 299–308 (Sept. 2018).

555 35. Luo, Y. *et al.* Exploration of Resting-state Brain Functional Connectivity as Pre-
556 clinical Markers for Arousal Prediction in Prolonged Disorders of Consciousness: A
557 Pilot Study Based on Functional Near-infrared Spectroscopy. *Brain and Behavior*
558 **14,** e70002 (Aug. 2024).

559 36. Vogt, B. A. Midcingulate Cortex: Structure, Connections, Homologies, Functions
560 and Diseases. *Journal of Chemical Neuroanatomy* **74,** 28–46 (July 2016).

561 37. Bonhomme, V. *et al.* Resting-State Network-specific Breakdown of Functional Con-
562 nectivity during Ketamine Alteration of Consciousness in Volunteers. *Anesthesiology*
563 **125,** 873–888 (Nov. 2016).

564 38. Peng, X. *et al.* Robust Dynamic Brain Coactivation States Estimated in Individuals.
565 *Science Advances* **9,** eabq8566 (Jan. 2023).

566 39. Paquola, C. *et al.* The Architecture of the Human Default Mode Network Explored
567 through Cytoarchitecture, Wiring and Signal Flow. *Nature Neuroscience* **28,** 654–
568 664 (Mar. 2025).

569 40. Greicius, M. D. *et al.* Resting-State Functional Connectivity Reflects Structural Con-
570 nectivity in the Default Mode Network. *Cerebral Cortex (New York, N.Y.: 1991)* **19,**
571 72–78 (Jan. 2009).

572 41. Jitsuishi, T. & Yamaguchi, A. Characteristic Cortico-Cortical Connection Profile of
573 Human Precuneus Revealed by Probabilistic Tractography. *Scientific Reports* **13,**
574 1936 (Feb. 2023).

575 42. Khalsa, S. *et al.* The Structural and Functional Connectivity of the Posterior Cin-
576 gulate Cortex: Comparison between Deterministic and Probabilistic Tractography
577 for the Investigation of Structure-Function Relationships. *NeuroImage* **102 Pt 1,**
578 118–127 (Nov. 2014).

579 43. Parvizi, J. *et al.* Neural Connections of the Posteromedial Cortex in the Macaque.
580 *Proceedings of the National Academy of Sciences of the United States of America*
581 **103,** 1563–1568 (Jan. 2006).

582 44. Passarelli, L. *et al.* Uniformity and Diversity of Cortical Projections to Precuneate
583 Areas in the Macaque Monkey: What Defines Area PGm? *Cerebral Cortex* **28,** 1700–
584 1717 (May 2018).

585 45. Cunningham, S. I. *et al.* Structural and Functional Connectivity of the Precuneus
586 and Thalamus to the Default Mode Network. *Human Brain Mapping* **38,** 938–956
587 (2017).

588 46. Buckwalter, J. A. *et al.* Thalamic Projections to the Posteromedial Cortex in the
589 Macaque. *The Journal of comparative neurology* **507,** 1709–1733 (Apr. 2008).

590 47. Farzampour, Z. & Huguenard, J. Seizing upon Mechanisms for Impaired Conscious-
591 ness. *Neuron* **85,** 453–455 (Feb. 2015).

48. Vollenweider, F. X. & Geyer, M. A. A Systems Model of Altered Consciousness: Integrating Natural and Drug-Induced Psychoses. *Brain Research Bulletin. Serotonin: From the Molecule to the Clinic* **56,** 495–507 (Nov. 2001).

49. Danielson, N. B. *et al.* The Default Mode Network and Altered Consciousness in Epilepsy. *Behavioural Neurology* **24,** 55–65 (2011).

50. Amico, E. *et al.* Posterior Cingulate Cortex-Related Co-Activation Patterns: A Resting State fMRI Study in Propofol-Induced Loss of Consciousness. *PLOS ONE* **9,** e100012 (June 2014).

51. Boveroux, P. *et al.* Breakdown of Within- and between-Network Resting State Functional Magnetic Resonance Imaging Connectivity during Propofol-Induced Loss of Consciousness. *Anesthesiology* **113,** 1038–1053 (Nov. 2010).

52. Willbrand, E. H. *et al.* Uncovering a Tripartite Landmark in Posterior Cingulate Cortex. *Science Advances* **8,** eabn9516 (Sept. 2022).

53. Pinheiro-Chagas, P. *et al.* Direct Intracranial Recordings in the Human Angular Gyrus during Arithmetic Processing. *Brain Structure and Function* (July 2022).

54. Dosenbach, N. U. F. *et al.* The Brain's Action-Mode Network. *Nature Reviews Neuroscience* (Jan. 2025).

55. Kaelen, M. *et al.* LSD Modulates Music-Induced Imagery via Changes in Parahippocampal Connectivity. *European Neuropsychopharmacology* **26,** 1099–1109 (July 2016).

56. Aliko, S. *et al.* A Naturalistic Neuroimaging Database for Understanding the Brain Using Ecological Stimuli. *Scientific Data* **7** (Oct. 2020).

57. Carhart-Harris, R. L. *et al.* Neural Correlates of the Psychedelic State as Determined by fMRI Studies with Psilocybin. *Proceedings of the National Academy of Sciences of the United States of America* **109,** 2138–2143 (Feb. 2012).

58. Dandash, O. *et al.* Selective Augmentation of Striatal Functional Connectivity Following NMDA Receptor Antagonism: Implications for Psychosis. *Neuropsychopharmacology: Official Publication of the American College of Neuropsychopharmacology* **40,** 622–631 (Feb. 2015).

59. Naci, L. *et al.* Functional Diversity of Brain Networks Supports Consciousness and Verbal Intelligence. *Scientific Reports* **8,** 13259 (Sept. 2018).

623 60. Stamatakis, E. A. *et al.* Changes in Resting Neural Connectivity during Propofol
624 Sedation. *PLOS ONE* **5,** e14224 (Dec. 2010).

Supplementary Materials

Datasets

LSD

The LSD dataset was shared by a previously published study. The data acquisition protocols were described in detail in this publication using the same dataset [55], so only a brief report a brief summary is provided here. Twenty healthy participants (4 female, mean age = 33±9 years, range = 22∼47 years) were scanned in two experimental conditions, separated by at least 2 weeks. On one of the visits, they were given a placebo (10-mL saline) and on the other they were given an active dose of LSD (75 μg of LSD in 10-mL saline). The order of receiving LSD or placebo was balanced across participants who were blinded to this order. The experiment for each condition consisted of three 7 min eyes-closed resting-state scanning sessions. In the second session, in-ear auditory stimulation (music) was given to the participants while being scanned.

The session using continuous music stimuli was taken into consideration for the following reasons. Firstly, we consider the benefit of increasing sample size outweighs the cost of increasing the heterogeneity in the data for the purpose of the current study, as the study is meant to capture the common (ir)regularities at a large spatiotemporal scale across heterogeneous datasets. Secondly, music listening is a variation of resting states, because participants in the music sessions also have uncontrolled, spontaneous thoughts, expect for being potentially guided by auditory cues. However, the resting-state sessions are not deprived of auditory stimuli. Furthermore, previous studies have shown that the FC patterns generated by naturalistic stimuli (including music, story narration and movie clips) can recapture the resting-state FC patterns while having a higher test-retest reliability than the resting state [56].

All imaging was performed on a 3T GE HDx system. The structural MRI scan was obtained in an axial orientation, with field of view = 256 × 256 × 192 and matrix = 256 × 256 × 192 to yield 1-mm isotropic voxel resolution, with a time-to-repetition (TR) of 7.9 ms, time-to-echo (TE) of 3.0 ms, inversion time of 450 ms and a flip angle of 20°. Functional images were acquired using a gradient echo planar imaging sequence, TR/TE = 2000/35 ms, field-of-view (FOV) = 220 mm, 64 × 64 acquisition matrix, parallel acceleration factor = 2, 90° flip angle. Thirty-five oblique axial slices were acquired in an interleaved fashion, each 3.4 mm thick with zero slice gap (3.4 mm isotropic voxels). The

precise length of each of the BOLD scans was 7:20 min.

Psilocybin (PSILO)

The PSILO dataset was shared by a previously published study. The data acquisition protocols were described in detail in a previous paper [57], so only a brief summary is provided here. Fifteen healthy participants (2 female, mean age = 32 years, SD = 8.9 years) underwent experiments that were designed in a similar way as the above LSD dataset acquisition. On one of the visits, they were given a placebo (10-mL saline) and on the other they were given an active dose of psilocybin (2 mg of psilocybin in 10-mL saline). The order of receiving psilocybin or placebo was randomised across participants who were blinded to this order. Each scanning session lasts for 18 min. Infusions began 6 min after the start of the scan.

All imaging was performed on a 3T GE HDx system. For every structural MRI scan, an initial 3D FSPGR scan in an axial orientation, with field of view = 256 × 256 × 192 and matrix = 256 × 256 × 192 to yield 1-mm isotropic voxel resolution (TR/TE = 7.9/3.0 ms; inversion time = 450 ms; flip angle = 20°). BOLD-weighted fMRI data were acquired using a gradient-echo EPI sequence, TR/TE = 3000/35 ms, field-of-view = 192 mm, 64 × 64 acquisition matrix, parallel acceleration factor = 2, 90° flip angle. Fifty-three oblique-axial slices were acquired in an interleaved fashion, each 3 mm thick with zero slice gap (3 × 3 × 3-mm voxels). A total of 240 volumes were acquired. There were each 100 volumes during the pre-injection and post-injection periods that were suggested to use for data analyses (i.e., 40 volumes during the injection were excluded). Reported results in the project were mainly generated from the post-injection dataset.

Ketamine (KETA)

The KETA dataset was shared by a previously published study. The data acquisition protocols were described in detail in a previous paper [58], so only a brief summary is provided here. Twenty-one young healthy participants (11 female, mean age = 28.7 years, SD = 3.2 years) were recruited to participate in the experiment which involved two conditions separated by at least 1 week. On one occasion, they received a continuous computer-controlled intravenous infusion of a racemic ketamine solution (2mg/ml) until a targeted plasma concentration of 100 ng/ml was reached, on the other occasion, saline infusion was administered. Infusion order was randomly counterbalanced across partici-

pants. Participants were instructed to close their eyes and let the minds wander without going to sleep.

All imaging was performed on a 3.0 T MRI scanner (Siemens Magnetom, Trio Tim, Erlangen, Germany) equipped with a 12-channel array coil located at the Wolfson Brain Imaging Centre, Addenbrooke's Hospital, Cambridge, UK. For every structural MRI scan, high-resolution anatomical T_1 images were acquired using a three-dimensional magnetic-prepared rapid gradient echo (MPPRAGE) sequence. 176 contiguous sagittal slices (1.0 mm thickness, TR = 2300 ms, TE = 2.98 ms, flip angle = 91°, FOV = 256 mm in 240 × 256 matrix) were acquired with a voxel size of 1.0 mm3. For functional MRI data, T_2^*-weighted echo-planar images (3 × 3 × 3.75 mm voxel size, TR = 2000 ms, TE = 30 ms, flip angle of 78° in 64 × 64 matrix size, and 240 mm FOV) were acquired under eyes-closed resting-state conditions. Imaging parameters were. A total of 300 volumes comprising 32 slices each were obtained.

Propofol-London Ontario site (PPFL-L)

The PPFL-L dataset was shared by a previously published study. The data acquisition protocols were described in detail in a previous paper [59], so only a brief summary is provided here. Nineteen (6 female, 18–40 years) healthy participants were recruited. During scanning, participants were asked to close eyes and not fall asleep, during which, a 5-min continuous audio story was presented to the participants. An 8-min resting state scanning was also acquired. The audio story and resting state scanning were both acquired while participants were awake (non-sedated) and deeply anaesthetised with propofol (Ramsay score 5). Both sessions were taken into analyses for the aforementioned reasons (detailed in the paragraphs for introducing the LSD dataset). Ramsay level 5 was considered achieved once participants stopped responding to verbal commands and were rousable only to physical stimulation. The mean estimated effect-site propofol concentration was 2.48 (1.82–3.14) μg/ml, and the mean estimated plasma propofol concentration was 2.68 (1.92–3.44) μg/ml. Mean total mass of propofol administered was 486.58 (373.30–599.86) mg.

All imaging was performed on a 3 Tesla Siemens Tim Trio system, with a 32-channel head coil. Structural MRI scans were obtained using a T1-weighted 3D MPRAGE sequence (32 channel coil, voxel size: 1 × 1 × 1 mm, acquisition time = 5 minutes and 38 seconds, TE = 4.25 ms, matrix size = 240 × 256 × 192, flip angle = 9°). For functional

MRI, echo-planar images were acquired (33 slices, voxel size: 3 × 3 × 3, inter-slice gap of 25%, TR = 2000 ms, TE = 30 ms, matrix size = 64 × 64, flip angle = 75°). The audio story and resting state scanning had 155 and 256 volumes, respectively.

Propofol-Cambridge site (PPFL-C)

We have collected the PPFL-C dataset and published it for a different study in a previous paper [60], so only a brief summary is provided here. Twenty-five participants (mean = 34.62 years, SD = 9.05 years, range = 19-52 years) recruited to the study. During scanning, participants were instructed to "keep their eyes closed and think of nothing in particular". Propofol was administered using a computer controlled intravenous infusion aiming to achieve three target plasma levels: no drug (awake) and 1.2 μg/ml (moderate sedation). At regular intervals between scans, depth of sedation was evaluated by assessing the participants' responsiveness to verbal instructions. Only awake and moderate conditions were included for further analyses in this project.

All imaging was performed on a Siemens Trio 3T scanner (WBIC, Cambridge). T1-weighted structural images were also acquired at 1 mm isotropic resolution in the sagittal plane, using an MPRAGE sequence with TR = 2250 ms, inversion time (TI) = 900 ms, TE = 2.99 ms and flip angle = 9°. Each functional BOLD volume consisted of 32 interleaved, descending, oblique axial slices, 3 mm thick with interslice gap of 0.75 mm and in-plane resolution of 3 mm, field of view = 192 × 192 mm, repetition time = 2 s, acquisition time = 2 s, time echo = 30 ms, and flip angle = 78°. A total of 150 volumes of resting state fMRI were acquired at each level of sedation in a period of 5 min.

Spatial localisation of the regions of interest

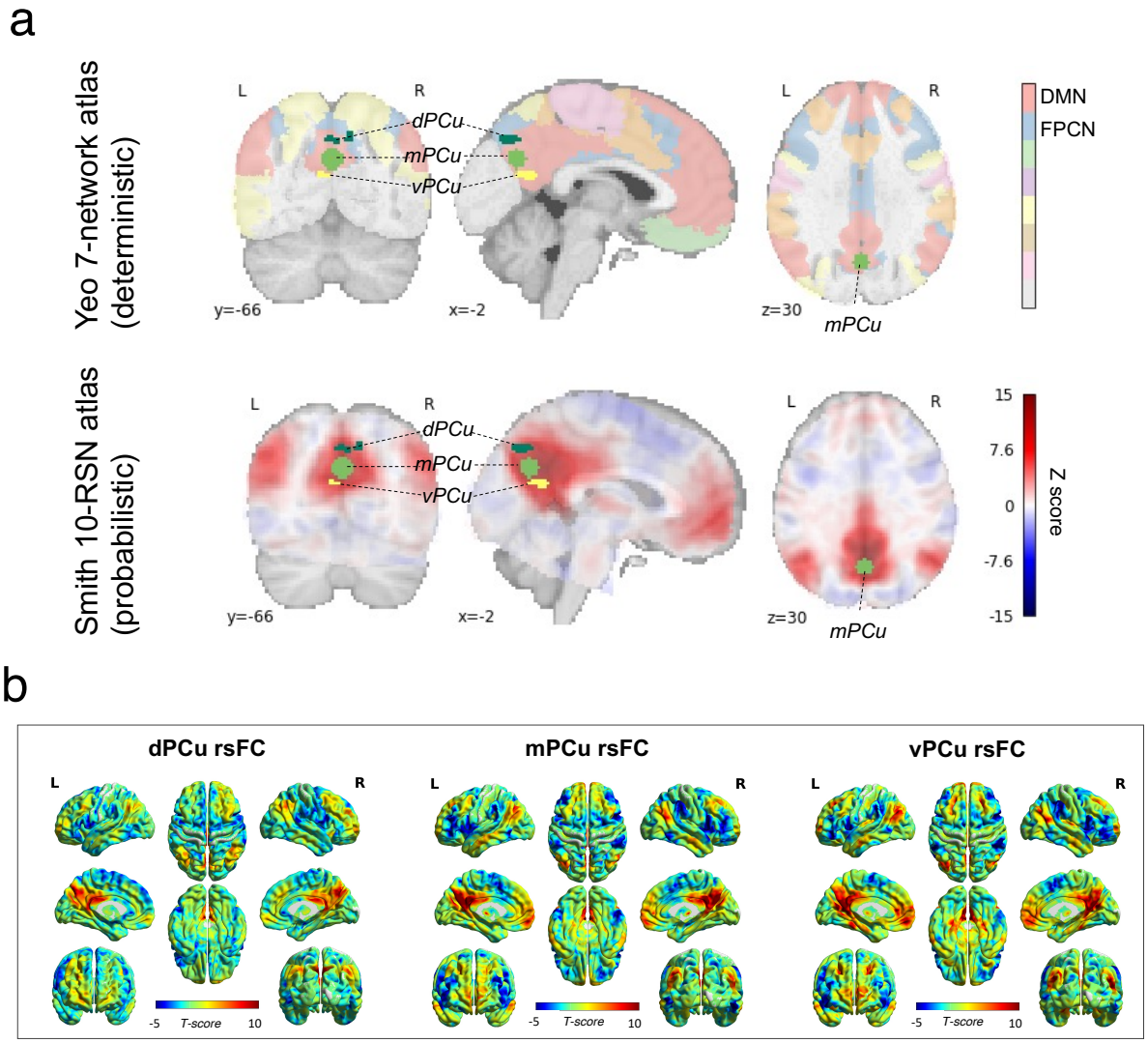
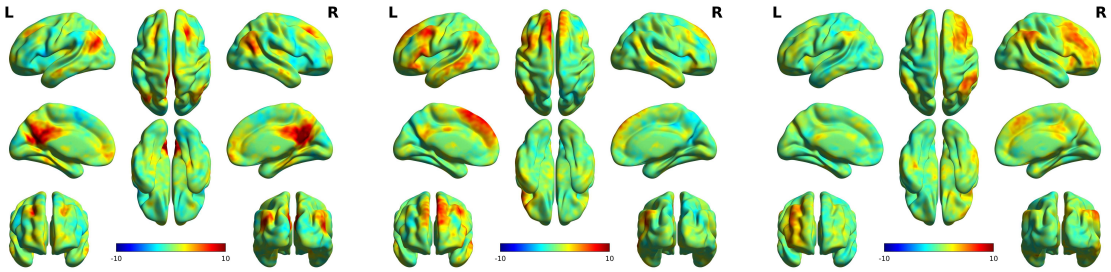


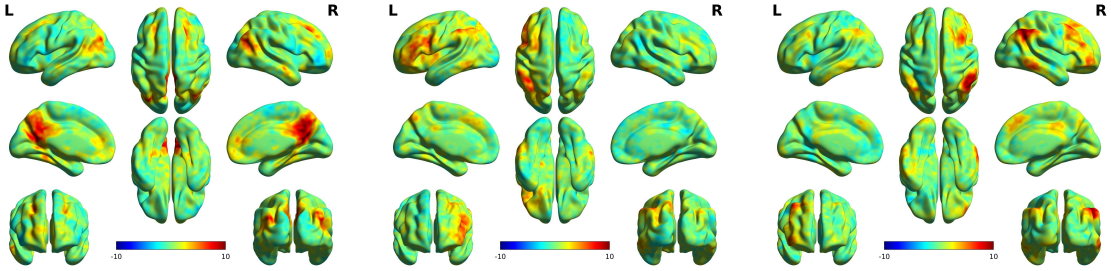
Figure S1: Spatial localisation of the regions of interest (dPCu, mPCu, vPCu). (a) The coronal, sagittal and horizontal view of the ROIs, overlapped with network atlases. The upper panel shows the ROIs' spatial localisation overlapped with the *Yeo2011* 7-network. The lower panel shows the ROIs spatial localisation overlapped with the *Smith2009* 10-RSN atlas (probabilistic). The red regions in both panels indicate the DMN. (b) Seed-based FC of d/m/vPCu. Resting-state FC in healthy awake participants revealed that the d/m/vPCu have similar positive connectivity patterns, which all mainly cover the DMN territory; however, as we move from the dorsal to the ventral sections of the PCu, the differences among their FC patterns showed a spatial continuity, such that the connected area in the posterior parietal cortex seemed to "migrate" from the upper to the lower sulcus of the angular gyrus (AG), and the ventro-medial prefrontal cortex (vmPFC) and the anterior cingulate cortex (ACC) get progressively more connected.

Supplementary figures for the group-specific ICA components



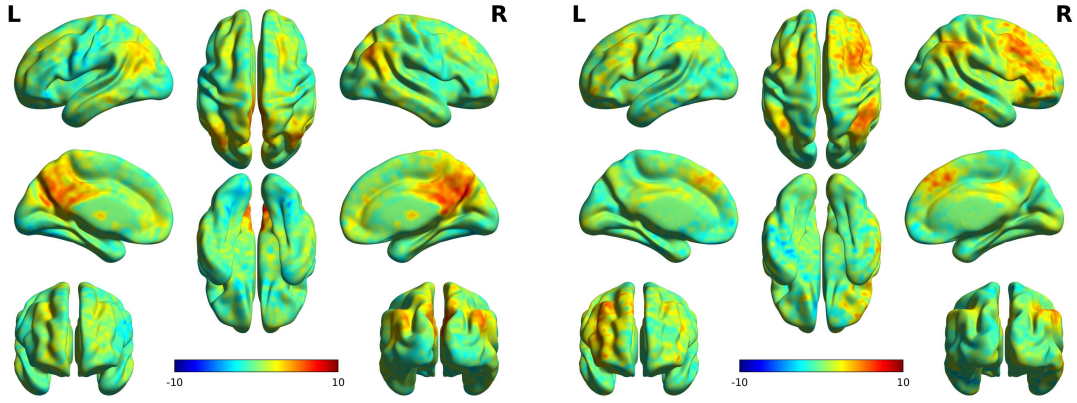
(a) DMN (b) lFPCN (c) rFPCN

Figure S2: Independent components identified as the DMN and FPCN in the LSD (placebo) dataset



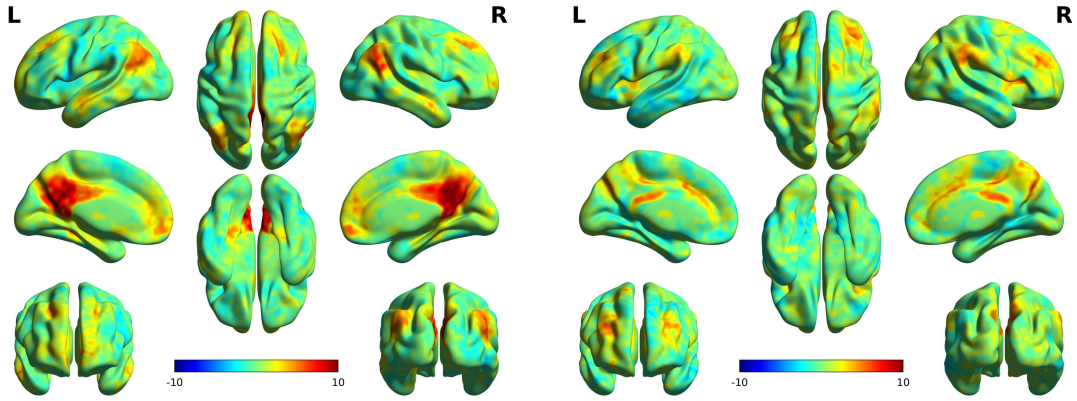
(a) DMN (b) lFPCN (c) rFPCN

Figure S3: Independent components identified as the DMN and FPCN in the PSILO (placebo) dataset



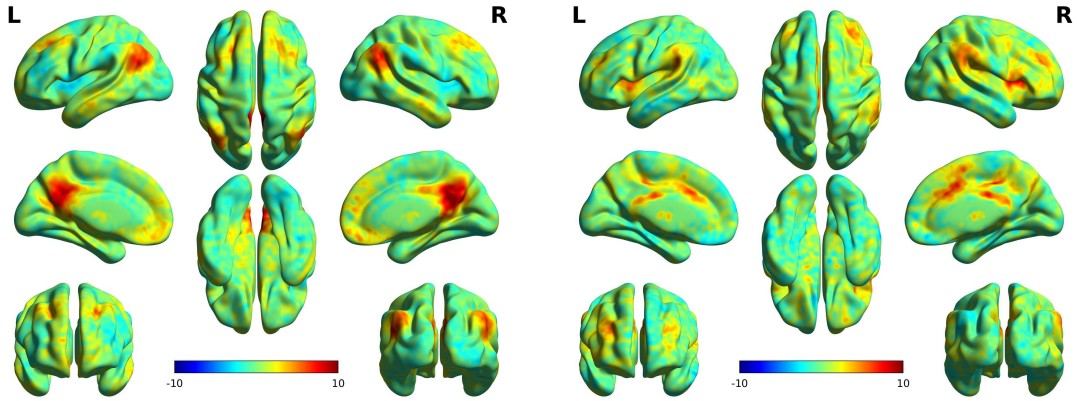
(a) DMN (b) FPCN

Figure S4: Independent components identified as the DMN and FPCN in the PSILO (placebo) dataset



(a) DMN (b) FPCN

Figure S5: Independent components identified as the DMN and FPCN in the PPFL-London (placebo) dataset



(a) DMN (b) FPCN

Figure S6: Independent components identified as the DMN and FPCN in the PPFL-Cambridge (placebo) dataset

Spatial entropy

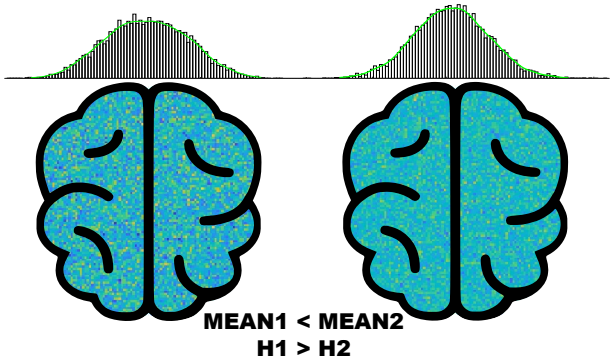


Figure S7: **Illustration of spatial entropy (H).** The first distribution compared to the second distribution of data has a smaller mean but a bigger H (i.e., spatial entropy). As visualised by the coloured pixels corresponding to the data, the first cartoon image looks more patchy and scattered than the other one. We hypothesise that psychedelic ASC is different than sedative ASC for having higher spatial entropy, despite similarly having reduced FGp.

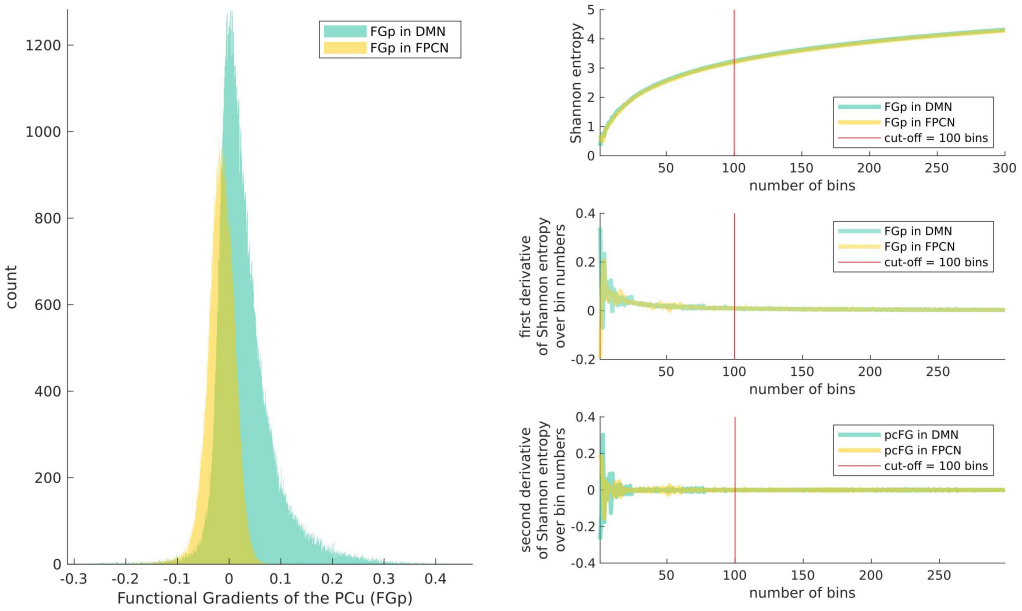


Figure S8: Shannon entropy over different bin numbers to use. The distribution of data was averaged FGp across participants from all datasets.

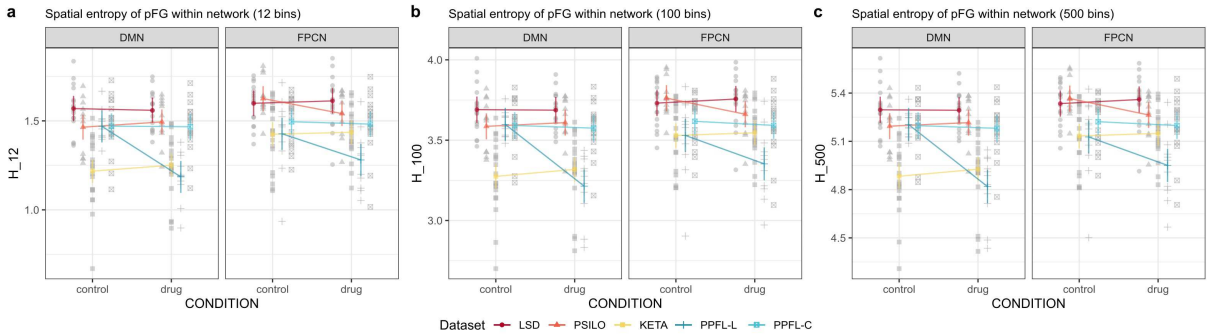


Figure S9: Group comparisons of the spatial entropy using different bin numbers. Bin numbers of 12 and 500 were used as alternatives to show that the presented results about spatial entropy is not contingent on the chosen bin number 100. 12 was chosen as a lower bound because with this bin number, the bin size is equivalent to a unit of standard deviation of the group-averaged FGp distribution in both networks.

Significance testing results

Table S1: **Significance table for the statistical testing of the differences in the precuneal functional gradient (FGp)) between drug and control conditions for all the datasets.**The null hypothesis is that there is no difference of FGp between conditions, while the alternative hypothesis is that the FGp in the DMN or FPCN mask are diminished under the drug-induced altered states of consciousness. One-tailed permutation tests were performed independently for each dataset, each FC type and each network. P values for statistical inferences were family-wise corrected for the multiple comparisons. The auditory stimuli for the LSD dataset was music, while that for the PPFL-L dataset was story narration.

Dataset	Session(s)	FC type	Network	T	crit. T	P_{corr}	Sig.	DF
LSD	rest+audio	a	DMN	-36.94	-2.34	0.00	1	27003
LSD	rest+audio	a	FPCN	-50.07	-2.31	0.00	1	19833
LSD	rest+audio	+	DMN	-35.66	-2.34	0.00	1	27003
LSD	rest+audio	+	FPCN	-40.12	-2.31	0.00	1	19833
LSD	rest+audio	-	DMN	-8.98	-2.34	0.00	1	27003
LSD	rest+audio	-	FPCN	-52.96	-2.31	0.00	1	19833
LSD	rest	a	DMN	-87.84	-2.34	0.00	1	27003
LSD	rest	a	FPCN	-19.42	-2.31	0.00	1	19833
LSD	rest	+	DMN	-72.78	-2.34	0.00	1	27003
LSD	rest	+	FPCN	-48.58	-2.31	0.00	1	19833
LSD	rest	-	DMN	-64.33	-2.34	0.00	1	27003
LSD	rest	-	FPCN	-7.50	-2.31	0.00	1	19833

Continued on next page

Table S1 – continued from previous page

Dataset	Session(s)	FC type	Network	T	crit. T	P_{corr}	Sig.	DF
LSD	audio	a	DMN	44.39	-2.34	1.00	0	27003
LSD	audio	a	FPCN	-47.16	-2.31	0.00	1	19833
LSD	audio	+	DMN	37.66	-2.34	1.00	0	27003
LSD	audio	+	FPCN	-27.18	-2.31	0.00	1	19833
LSD	audio	-	DMN	23.35	-2.34	1.00	0	27003
LSD	audio	-	FPCN	-53.61	-2.31	0.00	1	19833
PSILO	rest	a	DMN	-17.88	-2.35	0.00	1	28701
PSILO	rest	a	FPCN	-69.38	-2.36	0.00	1	16933
PSILO	rest	+	DMN	-8.78	-2.35	0.00	1	28701
PSILO	rest	+	FPCN	-54.37	-2.36	0.00	1	16933
PSILO	rest	-	DMN	12.17	-2.35	1.00	0	28701
PSILO	rest	-	FPCN	-69.38	-2.36	0.00	1	16933
KETA	rest	a	DMN	-13.39	-1.97	0.00	1	39032
KETA	rest	a	FPCN	-22.21	-2.00	0.00	1	18844
KETA	rest	+	DMN	-9.80	-1.97	0.00	1	39032
KETA	rest	+	FPCN	-46.04	-2.00	0.00	1	18844
KETA	rest	-	DMN	-37.46	-1.97	0.00	1	39032
KETA	rest	-	FPCN	0.96	-2.00	0.71	0	18844
PPFL-L	rest+audio	a	DMN	-120.59	-2.38	0.00	1	26745
PPFL-L	rest+audio	a	FPCN	-130.64	-2.31	0.00	1	12058
PPFL-L	rest+audio	+	DMN	-134.78	-2.38	0.00	1	26745
PPFL-L	rest+audio	+	FPCN	-46.38	-2.31	0.00	1	12058
PPFL-L	rest+audio	-	DMN	-18.59	-2.38	0.00	1	26745
PPFL-L	rest+audio	-	FPCN	-140.74	-2.31	0.00	1	12058
PPFL-L	rest	a	DMN	-62.76	-2.38	0.00	1	26745
PPFL-L	rest	a	FPCN	-85.81	-2.31	0.00	1	12058
PPFL-L	rest	+	DMN	-99.23	-2.38	0.00	1	26745
PPFL-L	rest	+	FPCN	31.16	-2.31	1.00	0	12058
PPFL-L	rest	-	DMN	89.15	-2.38	1.00	0	26745
PPFL-L	rest	-	FPCN	-152.64	-2.31	0.00	1	12058
PPFL-L	audio	a	DMN	-126.13	-2.38	0.00	1	26745

Continued on next page

Table S1 – continued from previous page

Dataset	Session(s)	FC type	Network	T	crit. T	P_{corr}	Sig.	DF
PPFL-L	audio	a	FPCN	-134.32	-2.31	0.00	1	12058
PPFL-L	audio	+	DMN	-119.33	-2.38	0.00	1	26745
PPFL-L	audio	+	FPCN	-101.69	-2.31	0.00	1	12058
PPFL-L	audio	-	DMN	-72.02	-2.38	0.00	1	26745
PPFL-L	audio	-	FPCN	-103.23	-2.31	0.00	1	12058
PPFL-C	rest	a	DMN	-45.14	-1.96	0.00	1	22533
PPFL-C	rest	a	FPCN	-5.40	-1.95	0.00	1	21377
PPFL-C	rest	+	DMN	-57.73	-1.96	0.00	1	22533
PPFL-C	rest	+	FPCN	1.75	-1.95	0.93	0	21377
PPFL-C	rest	-	DMN	-21.10	-1.96	0.00	1	22533
PPFL-C	rest	-	FPCN	-9.21	-1.95	0.00	1	21377

a: all; +: positive; -: negative ;

crit. T: critical T-value for 95% confidence;

P_{corr}: Family-wise error rate corrected P value;

Sig.: significance decision;

DF: degrees of freedom;